Room temperature gravitational wave bar detector with optomechanical readout

L. Conti[a)]
INFN, Sezione di Padova and Dipartimento di Fisica, Università di Padova Via Marzolo 8, I-35131 Padova, Italy

M. De Rosa and F. Marin
INFN, Sezione di Firenze and Dipartimento di Fisica, Università di Firenze, and LENS Via Sansone 1, I-50019 Sesto Fiorentino (Firenze), Italy

L. Taffarello
INFN, Sezione di Padova, Via Marzolo 8, I-35131 Padova, Italy

M. Cerdonio
INFN, Sezione di Padova and Dipartimento di Fisica, Università di Padova Via Marzolo 8, I-35131 Padova, Italy

(Received 26 August 2002; accepted 12 December 2002)

We present the full implementation of a room-temperature gravitational wave bar detector equipped with an optomechanical readout. The bar mechanical vibrations are read by a Fabry–Pérot interferometer whose length changes are compared with a stable reference optical cavity by means of a resonant laser. The detector performance is completely characterized in terms of spectral sensitivity and statistical properties of the fluctuations in the system output signal. This kind of readout technique allows for wide-band detection sensitivity and we can accurately test the model of the coupled oscillators for thermal noise. Our results are very promising for cryogenic operation and represent an important step towards significant improvements in the performance of massive gravitational wave detectors. © *2003 American Institute of Physics.* [DOI: 10.1063/1.1544077]

I. INTRODUCTION

The direct observation of gravitational waves (GWs) is one of the most challenging tasks for experimental physics. The effort devoted to this goal started in the 1960's, based on theoretical predictions of the expected signal, which are now considered as very optimistic.[1] The experimental strategy for detecting GW signals was based initially on massive acoustic detectors[2] and nowadays continues with long base line interferometers.[3–6] The former are the most sensitive GW detectors presently active[7] and they offer interesting possibilities for future advanced versions.[8,9]

Cryogenic bar detectors are currently equipped with resonant capacitive or inductive transducers followed by superconducting quantum interference device (SQUID) amplifiers or by a microwave resonant cavity. The sensitivity is presently limited by the amplification stage that operates $\sim 10^4$ times above the standard quantum limit,[10] giving a bandwidth of a few hertz around the two mechanical vibration modes of the coupled oscillators system.

The possibility of using optical techniques for the readout of bar vibrations was early considered by Drever.[11] Kulagin *et al.*[12] theoretically studied the possibilities of an optical readout system for a Weber bar with resonant mechanical transformer. This idea was developed by Richard,[13] who designed and theoretically investigated in detail such a system.[14] Richard and co-workers also tested at room temperature an optomechanical transducer made by a Fabry–Pérot cavity installed on a double oscillator, observing a rms displacement noise consistent with the calculated thermal fluctuations.[15]

At this point, there has been no experimental test of a massive bar detector instrumented with a resonant optical trasducer. On the other hand, the technology has much advanced during the last years in the fields of laser stabilization and fabrication of optical components. As a consequence, the expected characteristics of an optical readout system are even more promising and could result in a major advance for GW massive detectors.

In the framework of the AURIGA collaboration[16,17] we are developing a complete optical readout system for ultracryogenic bar detectors.[18] The basic idea is to use a high-finesse Fabry–Pérot cavity between the bar and a resonant mechanical transducer and then to compare the length of this optical resonator, possibly carrying a GW signal, with that of a stable reference cavity by means of a resonant laser.

In this work was present a room temperature GW bar detector operating with a resonant optical readout system. The detector performance is completely characterized in terms of its spectral sensitivity and the statistical properties of the fluctuations in the system output signal. Our apparatus represents a wide-band (several tens of hertz) GW acoustic detector which is limited by thermal noise at least in the frequency range of highest sensitivity. Thanks to this property, we can accurately study the output spectrum of the thermal noise and we show that the description of the bar and

a)Electronic address: conti@lnl.infn.it

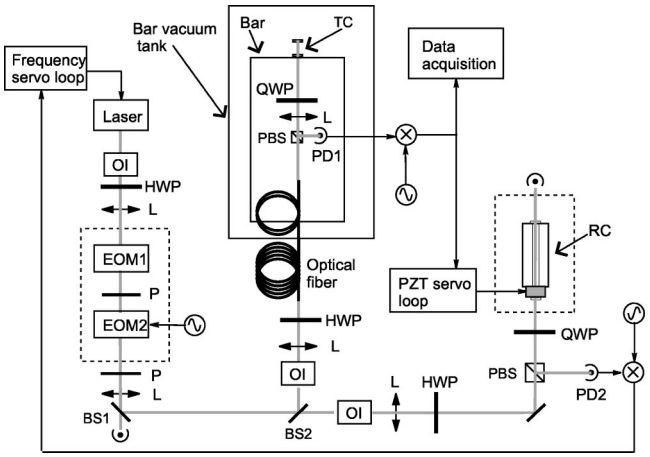

FIG. 1. Experimental setup: the drawing is not to scale. OI: optical isolator; HWP: half-wave plate: QWP: quarter-wave plate; *L*: lens; EOM1, EOM2: electro-optic modulators; *P*: polarizer; BS1, BS2: beam-splitters; PBS: polarizing beam-splitter; PD1, PD2: photodiodes; RC: reference cavity; TC: transducer cavity. Dashed lines mark out active thermal stabilization.

transducer coupled oscillators cannot be given in terms of decoupled normal modes, as usually assumed.

The outline of this article is the following. In Sec. II we describe the experimental apparatus, and in particular the readout system. In Sec. III A we present the mechanical characteristics and the displacement noise of the detector, as deduced from the output signal. The thermal noise in the output spectrum is analyzed in Sec. III B. Then we investigate the statistical properties of the output fluctuations, performing the detailed analysis required to characterize a GW detector (Sec. III C). Finally in Sec. III D we estimate the sensitivity of the bar as GW detector.

II. THE READOUT SYSTEM

A schematic drawing of the room-temperature GW detector equipped with the optomechanical readout is shown in Fig. 1. The mechanical vibrations of the bar are amplified by a coupled mechanical oscillator and transformed into length changes of an optical cavity, hereafter called transducer cavity (TC). The readout system is composed of a laser source, frequency stabilized to a reference cavity (RC), a set of optical fibers and components to convey the radiation to TC and the optoelectronics for signal detection and processing.

The bar is a 3 m long, 2300 kg cylinder made of Al5056. Its first longitudinal vibration mode, useful for GW detection, resonates at 875 Hz, when no load is applied. The measured resonant frequency decreases by -0.38 Hz/kg when the trasducer nonresonant mass is attached to the bar end faces, giving a calculated frequency of $\nu_b = 866$ Hz when the bar is operated with the full readout system. The mechanical quality factor of the resonance is 1.8×10^5 and is measured from the decay time of the excited vibration. The bar is kept in a vacuum chamber, placed a few meters apart from the optical table, and it is isolated from floor mechanical noise by a cascade of passive filters which achieve an overall vertical isolation of about -140 dB at the bar frequency, as sensed at the bar middle section. During the work reported here the vacuum system, including a roots pump backed by a rotary pump, was operated for about 1 h per day only.

The output beam of a commercial neodymium-doped yttritium-aluminum-garnet (Nd:YAG) laser source, emitting 50 mW at 1.064 μm, passes through an optical isolator and two electro-optic modulators (EOMs) enclosed in a thermally stabilized enclosure. The first EOM is used with a polarizer in an amplitude stabilization loop. The purpose of this noise eater, described in detail in Ref. 19, is to reduce the effect of the backaction on the transducer, but it is not relevant for the work reported here. The second EOM is a resonant modulator working at 13.3 MHz which accomplishes phase modulation with a depth of about 1 rad. A first beam-splitter (BS1) transmits 20% of the radiation for the noise eater, while the reflected beam is directed towards a second 70% transmission beam splitter (BS2). The reflected beam, after an optical isolator, is coupled to a single-mode polarization-maintaining fiber and arrives to a 135 $\times 340$ mm^2 Al plate anchored to the bar middle section.

The optical fiber is formed by joining 4 patchcords with FC/PC connectors, for a total length of 13 m, and includes a homemade vacuum feedthrough. The two fiber ends have pigtailed collimators, with antireflection coating. The overall power transmission of the fiber assembly is about 50%.

The 1.5 mW collimated beam transmitted by the fiber passes through an optical circulator, formed by a polarizing beam splitter plus a quarter-wave plate, and a telescope to properly couple the radiation to the TEM_{00} mode of TC. Four tilting mirrors send the beam towards the transducer cavity on the bar end face. The beam reflected by TC, after the circulator, is detected by a photodiode (PD1). The TC is a 6 mm long Fabry–Pérot cavity, with a finesse of 28 000, formed by an input concave mirror (radius of curvature 1 m, diameter 0.5″) glued to a support fixed to the bar, and a flat back mirror (diameter 0.5″) glued to the oscillating mass of the mechanical transducer. This resonant transducer is machined from a single piece of Al5056 and it is composed of a thin circular plate loaded by a central 1.25 kg inert mass. The resonant frequency of the first drum mode is about 882 Hz, according to the measurements described in Sec. III A. This resonator was designed for a previous version of the readout system and it is described in Ref. 18.

The beam transmitted by BS2, after an optical isolator and mode-matching lenses, is sent to a 110 mm long Fabry–Pérot reference cavity that has a finesse of 44 000. RC is formed by an Invar spacer with a couple of mirrors similar to the ones of the TC. The input flat mirror is glued on a piezoelectric actuator (PZT), which allows the tuning of the cavity length. The light power impinging on the cavity is about 4.5 mW. The cavity is kept in a vacuum chamber whose temperature is actively stabilized at about 34 °C within 0.1 °C. The beam reflected by this cavity is detected by a second photodiode (PD2) after an optical circulator.

The power level impinging on PD1 shows large variations: during the 42 h period of continuous data acquisition, it varied by up to 80%, on a time scale of typically a few hours. On the same period the power impinging on PD2 varied by less than 10%, with a longer time scale. The large variations sensed by PD1 are due to polarization fluctuations

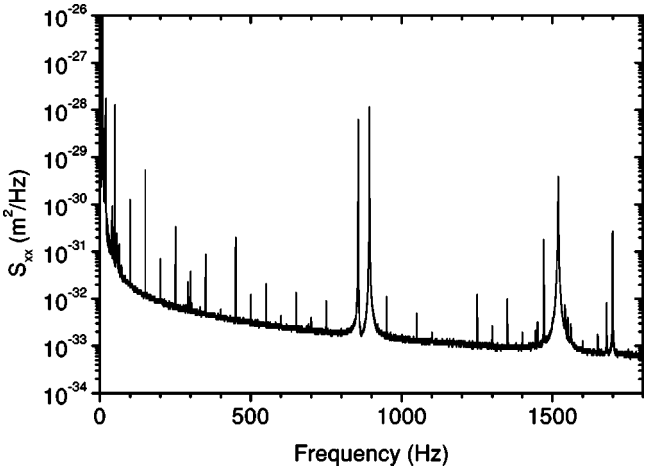

FIG. 2. Power spectral density S_{xx} of the displacement noise. The two peaks at 856 and 892 Hz correspond to the two mechanical modes of the coupled oscillators system formed by the bar first longitudinal mode and the transducer. Some other mechanical resonances are visible too. The sharp peaks at multiples of 50 Hz are due to the power line.

generated by drifts of the room temperature and originating from a nonperfect matching between the polarization axes of the fiber patchcords. They are turned into changes of the power impinging on TC by the optical circulator at the fiber output.

The ac component of the signals coming from the two photodiodes is demodulated at 13.3 MHz and filtered, according to the Pound–Drever scheme.[20] The resulting signals are used as discriminator for frequency locking and analysis. The laser frequency is locked to a resonance peak of RC with a servoloop which has a unit gain frequency of 30 kHz. The loop gain is maximized in the frequency range between 600 and 900 Hz, where it reaches 120 dB, and allows to achieve an in-loop frequency noise level below the shot noise limit. A detailed description of the loop electronics and performance can be found in Ref. 21. The resonant peak of RC is then superimposed to a resonance of TC by operating on the PZT actuator. The Pound–Drever signal from TC is used in a servoloop which drives the PZT through a low noise high-voltage amplifier. This low frequency servoloop has unity gain at about 1 Hz and allows the reference cavity to follow the resonance of TC in its thermal drifts. Due to the low loop bandwidth, the two cavities can be considered as free and independent in the frequency range of interest.

The same error signal from TC is acquired and analyzed to extract information concerning the motion of the bar detector.

III. EXPERIMENTAL RESULTS

A. Mechanical system and noise spectrum

The conversion of the detector output signal from voltage into length change of the transducer cavity is obtained using the slope of the corresponding error signal, measured with an accuracy of about 20%, and the known cavity length. The power spectral density S_{xx} of the displacement noise is shown in Fig. 2, which corresponds to the average of 1 h data. The peaks at 856 and 892 Hz correspond to the frequencies $\nu_{\pm}$ of the two mechanical modes of the coupled oscillators system formed by the bar and the resonant transducer. For the coupled system the following relation holds: $\nu_+\nu_- = \nu_b\nu_t$, where ν_t is the resonance frequency of the transducer. According to the value of $\nu_b = 866$ Hz calculated for the loaded bar we infer that the transducer resonance is at 882 Hz and thus detuned by $+16$ Hz with respect to the bar. A better coupling between the two oscillators is possible by adjusting the thickness of the transducer circular plate.

We determined the mechanical quality factor Q of the "+" and "−" modes by measuring the decay time of a resonant sinusoidal excitation applied to the bar by means of a piezoelectric actuator situated at the bar end face opposite the transducer. We got $Q_- = 16\,600$ and $Q_+ = 8700$. The factor of 2 of difference in the Qs is explained by considering that, due to the frequency detuning between the two resonators, the minus mode is more influenced by the (high Q) bar while the plus mode by the (low Q) transducer.

As it can be seen in Fig. 2, the peak spectral power in the modes exceeds by about 45 dB the background noise. The wide-band output noise of the optical readout system comes from the residual frequency fluctuations of the laser stabilized to RC and from the noise measured when the laser is far from the TC resonance. The laser frequency noise has been measured with respect to a stable Zerodur cavity, with an apparatus described in Ref. 22, and its effect gives a sensitivity limit as low as 2×10^{-2} Hz/$\sqrt{\text{Hz}}$ around 1 kHz. The far-from-resonance fluctuations are due to electronic noise, laser amplitude noise (including shot noise), and interference fringes. The overall effect gives a sensitivity limit of about 0.2 Hz/$\sqrt{\text{Hz}}$. The observed background, visible in Fig. 2, is about 20 dB higher than this limit and exhibits a decreasing behavior versus frequency.[23]

We fitted the noise power spectral density of 1 h output data with the function A/ν^{ϵ} between 75 and 1775 Hz, neglecting only the interval around the + and − modes and the resonance at 1519 Hz. We obtained $\epsilon = 1.16$ and $A = 4.2\times10^{-30}$ m^2 Hz$^{\epsilon}$/Hz. The origin of this noise is unknown and is presently under investigation. We remark that a $1/f$ frequency dependence in the noise spectrum is expected for the thermal noise of a mechanical oscillator with internal friction modeled as a constant imaginary part of the spring constant, in the frequency region below the oscillator resonance.

B. Thermal noise of the coupled oscillators system

A bar detector equipped with a resonant transducer is widely modeled as a system of two coupled harmonic oscillators and the output is often analyzed in terms of normal mode expansion. In particular, such assumption is used for studying the thermal noise of the system.[24] On the other hand, it has been suggested[25] and experimentally verified[26] that this description may fail if inhomogeneously distributed losses occur. For our system the condition for the validity of the normal mode expansion can be written, according to Ref. 25, as

$$\nu_b Q_b = \nu_t Q_t . \tag{1}$$

In our case, the large difference between the quality factors of the modes + and − can be brought back to a large difference in the effective Qs of the original oscillators Q_b and Q_t. Therefore, since the frequencies ν_b and ν_t are very similar, the condition of Eq. (1) is not satisfied.

We call x_b, m_b and x_t, m_t the coordinate and effective mass of the bar and transducer oscillator respectively, and f_b and f_t the corresponding total driving force. Assuming that only viscous damping is present, (we also considered the case of structural losses as dissipative mechanism, but no difference was found within the reported errors) the dynamics of the system is described by the equations of motion

$$\begin{cases} \ddot{x}_b + \dfrac{\omega_b}{Q_b}\dot{x}_b + \mu\dfrac{\omega_t}{Q_t}(\dot{x}_b - \dot{x}_t) + \omega_b^2 x_b + \mu\omega_t^2(x_b - x_t) \\ \qquad = \dfrac{f_b - f_t}{m_b} \\ \ddot{x}_t + \dfrac{\omega_t}{Q_t}(\dot{x}_t - \dot{x}_b) + \omega_t^2(x_t - x_b) = \dfrac{f_t}{m_t}, \end{cases}$$

where $\mu = m_t/m_b$ and $\omega_{b,t} = 2\pi\nu_{b,t}$. In the frequency domain the system can be written as

$$\mathbf{D}(\omega)\begin{pmatrix} X_b \\ X_t \end{pmatrix} = \begin{bmatrix} (F_b - F_t)/m_b \\ F_t/m_t \end{bmatrix}, \tag{2}$$

with

$$\mathbf{D}(\omega) = \begin{bmatrix} -\omega^2 + \omega_b^2 + \mu\omega_t^2 + i\omega\left(\dfrac{\omega_b}{Q_b} + \mu\dfrac{\omega_t}{Q_t}\right) & -\mu\omega_t^2 - i\mu\dfrac{\omega\omega_t}{Q_t} \\ -\omega_t^2 - i\dfrac{\omega\omega_t}{Q_t} & -\omega^2 + \omega_t^2 + i\dfrac{\omega\omega_t}{Q_t} \end{bmatrix},$$

where capital letters indicate Fourier transforms and i is the imaginary unit.

To simplify our analysis, in the following we consider the transducer cavity length changes as determined exclusively by a motion of the transducer. This is justified as the amplitude of a bar displacement is amplified at the transducer by a factor equal to $1/\sqrt{\mu}$, i.e., by a factor of about 30. We are thus interested to the noise power spectral density $S_{x_t x_t}$ of x_t which, if only stochastic thermal forces are present, can be written according to the Fluctuation–Dissipation theorem[25] as

$$S^T_{x_t x_t}(\omega) = \frac{2k_B T}{\omega^2}\mathrm{Re}[(i\omega\mathbf{D})^{-1}_{22}], \tag{3}$$

where k_B is the Boltzmann constant and T is the thermodynamic temperature. In order to account for the observed $\sim 1/f$ background, we add a phenomenological wide-band term

$$S_{x_t x_t}(\omega) = S^T_{x_t x_t}(\omega) + \frac{S_{\mathrm{WB}}}{\omega^{\epsilon}}. \tag{4}$$

We fitted the output spectrum using the expression of Eq. (4), in the frequency range between 780 and 950 Hz. The fit allows to infer the ratios Q_b/T, Q_t/T and the resonant frequencies ν_b, ν_t of the uncoupled oscillators, the effective mass m_t of the transducer oscillator and the magnitude S_{WB} of the background noise. The effective mass $m_b = 1180$ kg of the loaded bar resonator and the temperature T were kept constant during the fitting. We assumed that both oscillators are at the same thermodynamic temperature T of 296 K, as measured by a probe placed on the bar. This assumption seems reasonable at least for the bar as the inferred value for Q_b agrees very well with the one measured independently for the unloaded bar (1.8×10^5). The result of the fitting procedure is shown in Fig. 3 and the parameters are summarized in Table I. The two frequencies ν_b and ν_t agree well with the values estimated in Secs. II and III A. Also the scale factor S_{WB} of the background noise agrees with the value $(2\pi)^{\epsilon}A = 3.5\times10^{-29}$ m^2 Hz$^{\epsilon}$/Hz obtained in Sec. III A. As far as the transducer mass is concerned we notice that its effective mass deduced from the fit is greater than the mere 1.25 kg central mass.

We also attempted to fit the same data with the prediction of the normal mode expansion, as shown in Fig. 3. It is evident that, while the experimental spectrum is in excellent agreement with the model of Eqs. (3) and (4), the normal mode expansion fails to describe our system: the presence of inhomogeneously distributed losses causes the random fluctuations of the two initial oscillators to be correlated. The normal mode expansion overestimates the noise in between the two modes because it does not take into account such a correlation.

C. Statistical analysis of the output fluctuations

For a better understanding of the detection system, it is important to investigate the statistical behavior of the noise before attempting any estimation of its magnitude. In fact, one needs to be sure that the noise under observation follows the laws predicted for the expected noise sources. In particular, the fundamental hypothesis is that the noise is a (quasi-)stationary stochastic process with Gaussian statistics. The system statistics is a crucial issue for GW detectors and it can cause a dramatic decrease of the effective duty cycle. Indeed, it is safe to limit the analysis only to the periods when the experimental noise is well modeled, indicating that the detector is working properly.

The output of PD1 was recorded with an acquisition system identical to the one employed for the ultracryogenic GW

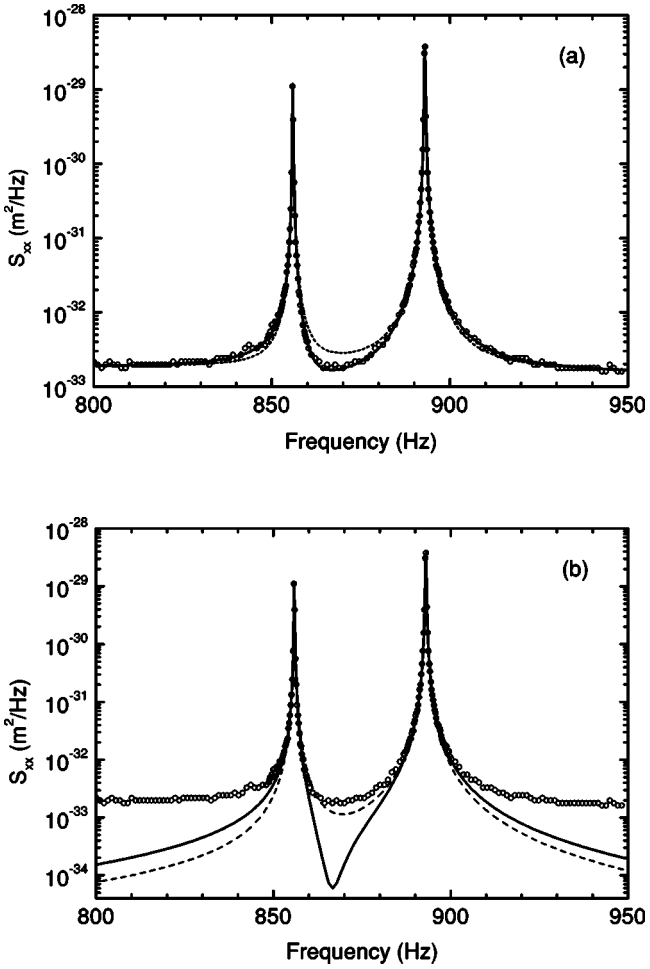

FIG. 3. (a) Power spectral density of the displacement noise. Circles: experimental data; solid line: fit according to the two-oscillators model of Eqs. (3) and (4); dashed line: fit according to the normal mode expansion. (b) The same as in (a), where the fitted curves are plotted without the wide-band $\sim 1/f$ contribution.

detector AURIGA: the data are sampled at 4.88 kHz and synchronized to UTC with a GPS clock. We have acquired data between May 31, 2001 and June 20, 2001. The data acquisition was not continuous due to intentional interruptions for diagnostic purposes and to system failures mainly originated by environmental temperature variations.[23] Manual relocking procedures require less than 15 min and the longest continuous locking period was 42 h. The overall data recording corresponds to 183 h. A few additional signals

TABLE I. Results of the fit of the experimental spectrum with Eqs. (3) and (4), assuming $T=296$ K for both resonators. The quoted errors (two standard deviations) refer to the last significant digit.

Parameter	Fitted value	Units
ν_b	866.31 (3)	Hz
ν_t	882.30 (3)	Hz
Q_b	1.8×10^5 (4)	
Q_t	6.60×10^3 (4)	
S_{WB}	3.5×10^{-29} (2)	$\mathrm{m^2\,Hz^{-\epsilon}/Hz}$
m_t	1.70 (2)	kg

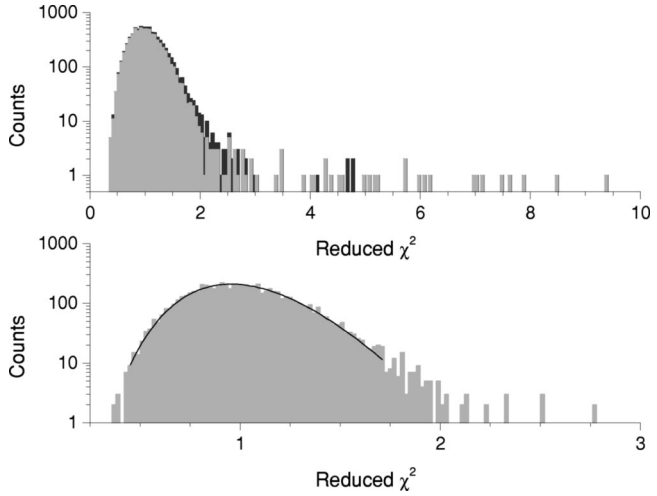

FIG. 4. Top: histogram of χ_a^2 of all triggers with SNR$>$4, before (dark gray) and after veto (light gray). Bottom: histogram of all triggers after veto and with 4$<$SNR$<$6. The solid line is the reduced χ^2 distribution with 30 degrees of freedom fitted to the vetoed data with 4$<$SNR$<$6. The data refer to June 9, 2001, and the veto is applied when vacuum pumps are on. The bins are 0.005 widen in χ_a^2.

were sampled at 20 Hz for monitoring the dc signals from PD1 and PD2, the temperature of the RC and the correction voltage fed to the PZT of the RC.

The acquired data were processed through the same data analysis used for the ultracryogenic detector.[27] The analysis implements a Wiener–Kolmogorov (WK) filter to search for δ-like signals (*triggers*), i.e., for short bursts whose Fourier transform can be considered as constant over the effective bandwidth of the detector. A maximum-hold algorithm is applied to the data and for each trigger we estimate the time of arrival, the amplitude and the χ^2 with respect to the expected shape. The latter discriminates a δ-like mechanical excitation of the bar, i.e., the GW signal, from spurious signals. The analysis also implements adaptive algorithms that update the parameters of the WK filter in order to follow slow drifts of the system.

In order to verify the Gaussian behavior of the detection output signal, we study the distribution of the reduced χ^2 (called χ_a^2 in the following) of all triggers found by the data analysis: for a random variable with Gaussian statistics χ_a^2 should follow a well-known distribution.[28] We focus on the 24 h of data acquired during June 9. The pumps that maintain the vacuum in the bar tank were switched on for 1 h, between h12.30 UTC and h13.30 UTC. We have vetoed the data acquired within this period in order to avoid the effect of the noise introduced by the pumps. We plot in Fig. 4 (top) the histogram of χ_a^2 of all triggers with signal-to-noise ratio (SNR) greater than 4,[29] before and after applying the veto (respectively, dark and light gray histogram). The tails at higher values of χ_a^2 are very efficiently cut away by considering only those triggers with 4$<$SNR$<$6 (bottom histogram). The number of degrees of freedom used to compute χ_a^2 is 30. We can well fit the data having 4$<$SNR$<$6, after veto, with the theoretical distribution of χ_a^2: the reduced χ^2 of the fit is 0.90.

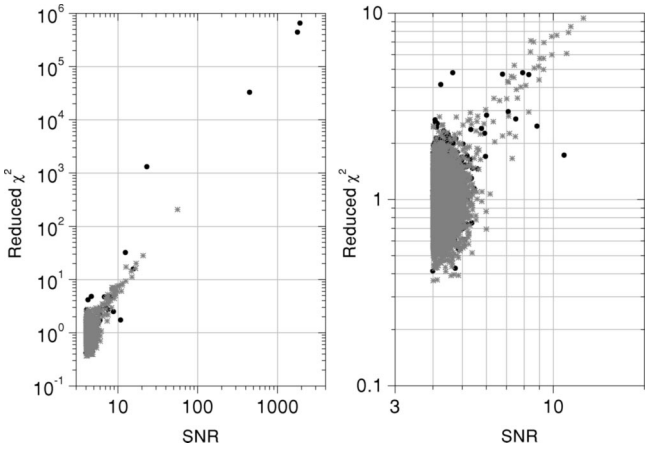

FIG. 5. Scatter plot of χ_a^2 vs SNR for all triggers after veto and with SNR >4 (gray stars). The closed circles correspond to the vetoed triggers. The data refers to June 9, 2001, and the veto is applied when the vacuum pumps are on.

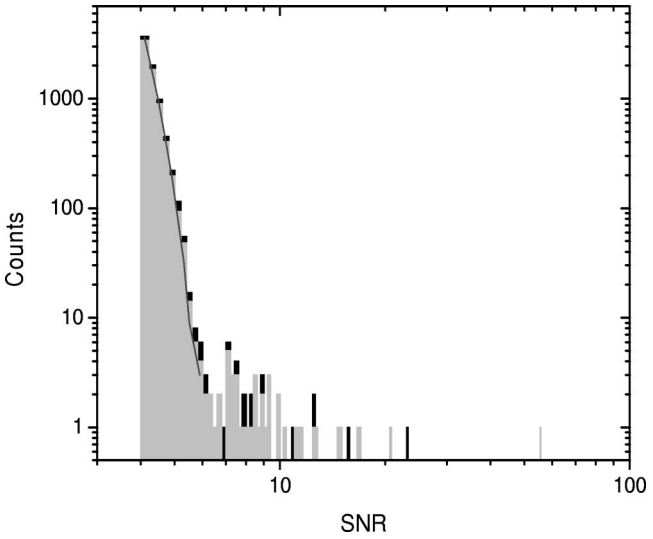

FIG. 6. Histogram of the SNR of all triggers with SNR>4, before (black) and after veto (light gray). The data refers to June 9, 2001, and the veto is applied when the vacuum pumps are on. The solid line is the distribution predicted by a numerical simulation of a Gaussian process with the same parameters as the detection system. The bins are 0.2 widen in SNR.

In Fig. 5 we plot the χ_a^2 of all triggers with SNR>4 versus the SNR. Most of them concentrate in the region of low SNR and $\chi_a^2<2$. A small fraction (about 0.05%) of triggers follows a linear law in the log–log plot of Fig. 5. Indeed, it has been shown[27] that a quadratic scale law of χ_a^2 versus the SNR is expected for signals which are not matched by the filter. 92% of triggers with SNR>6 surviving the veto can be rejected as they have a $\chi_a^2>2.1$, a threshold that corresponds to a confidence level of 3.9×10^{-4} for our 30 degrees of freedom.

An independent test of the Gaussian character of the system is the distribution of the SNR. In this case the analytical formula for the expected distribution involves the calculation of integrals that are not easily solvable. We therefore compare the experimental distribution of SNR with that obtained by simulating with Monte Carlo methods a Gaussian system having the same parameters as ours (namely, frequencies, bandwidth, and ratio between the height of the mechanical mode peaks and the background noise). The simulation output is passed through the same analysis as the real data, so that any deviation of our system from a Gaussian behavior would appear as a difference in the SNR distribution between the simulated and the true system. The results are plotted in Fig. 6 and the agreement is excellent, above all considering that 92% of the triggers at SNR>6 are rejected by the χ^2 test. The remaining signal distribution perfectly corresponds to the expected output of a system with Gaussian input noise, without any excess trigger.

D. Performance as GW detector

The sensitivity of the bar detector is determined from S_{hh}, defined as the spectral density of the total noise referred to the detector input and calibrated in terms of GW amplitude. Figure 7 shows $\sqrt{S_{hh}}$ in a neighborhood of the two modes $+$ and $-$. As expected, the best sensitivity is achieved close to the modes, with a peak at the mode $-$, that has a higher Q.

A critical parameter for a GW resonant detector is the detection bandwidth, which is particularly significant for the temporal definition of the candidate events and for the synchronization of several detectors.[30] The spectral sensitivity of the operating cryogenic bar detectors is characterized, with only one exception,[31] by narrow quasi-Lorentzian peaks, due to the relatively large amplifier noise. In that case, the detection bandwidth is of the order of a few hertz. For our detector, the sensitivity is relevant in the whole frequency interval between the modes, as expected for an optimized resonant transducer. The significant bandwidth exceeds the modes splitting. The output spectrum is asymmetric, but we remark that at 10 dB from the minimum the width is about 50 Hz.

The amplitude of a GW burst that would be detected with unitary SNR is $h_{\min}=3\times10^{-17}$. This is equivalent to a standard pulse of $0.8M_{\odot}c^2$ converted into GW at the distance of 10 kPc, i.e., at the galactic center. This performance is not of astrophysical interest, as expected for a room temperature operation, but it is very promising: once the system

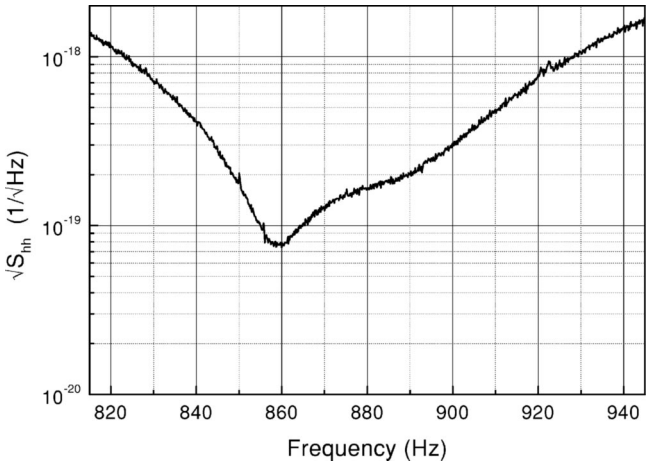

FIG. 7. Sensitivity of the GW detector, expressed in terms of the equivalent strain noise at the bar detector input. The data correspond to a 1 h average.

is upgraded both in the optics and in the detector design to operate at ultracryogenic temperatures, the sensitivity is expected to increase up to $h_{\min} \sim 10^{-20}$.

IV. CONCLUSIONS

We have operated a room temperature GW bar detector equipped with an optomechanical readout. The sensitivity is limited by thermal noise, due to the high operating temperature and low mechanical quality factors. Both parameters will improve in the case at cryogenic temperatures. The statistics of the detector noise is stable and Gaussian as expected. The sensitivity is enough to reveal the failure of the normal mode expansion in the presence of inhomogeneously distributed losses. The results achieved are a significant step towards the realization of an ultracryogenic resonant detector equipped with resonant optomechanical readout. This is projected to improve the bandwidth of the AURIGA detector by more than one order of magnitude from its current value.

ACKNOWLEDGMENTS

The authors gratefully acknowledge all the former and current components of the AURIGA group without whom this work would not have been done. They thank especially G. A. Prodi and J. P. Zendri for helping in the day by day laboratory work, L. Baggio, A. Ortolan and G. Vedovato for providing the data acquisition system and the data analysis tools and adapting them to our detector parameters, and S. Vitale for useful discussions and suggestions. This work was partially funded by the MURST (research program ''Transducer systems for cryogenic resonant detectors of gravitational waves'').

[1] G. E. Moss, L. R. Miller, and R. L. Forward, Appl. Opt. **10**, 2495 (1971); and references therein.
[2] P. Astone, Class. Quantum Grav. **19**, 1227 (2002).
[3] B. Willke *et al.*, Class. Quantum Grav. **19**, 1377 (2002).
[4] D. Sigg, Class. Quantum Grav. **19**, 1429 (2002).
[5] M. Ando and the TAMA collaboration, Class. Quantum Grav. **19**, 1409 (2002).
[6] F. Acernese *et al.*, Class. Quantum Grav. **19**, 1421 (2002).
[7] Z. A. Allen *et al.*, Phys. Rev. Lett. **85**, 5046 (2000); see also http://igec.lnl.infn.it/igec.
[8] E. Coccia, V. Fafone, G. Frossati, J. A. Lobo, and J. A. Ortega, Phys. Rev. D **57**, 2051 (1998).
[9] M. Cerdonio, L. Conti, J. A. Lobo, A. Ortolan, L. Taffarello, and J.-P. Zendri, Phys. Rev. Lett. **87**, 031101 (2001).
[10] H. Heffner, Proc. IRE **45**, 1604 (1962).
[11] R. W. P. Drever, J. Hough, W. A. Eldstein, J. P. Pugh, and W. Martin, in *Proceedings of the International Meeting of Experimental Gravitation*, edited by B. Bertotti (Atti Convegni de Lincei, Rome, 1977), Vol. 34, p. 365.
[12] V. V. Kulagin, A. G. Polnarev, and V. N. Rudenko, Sov. Phys. JETP **64**, 915 (1986).
[13] J.-P. Richard, J. Appl. Phys. **64**, 2202 (1988).
[14] J.-P. Richard, Phys. Rev. D **46**, 2309 (1992).
[15] Yi. Pang and J.-P. Richard, Appl. Opt. **34**, 4982 (1995).
[16] G. A. Prodi *et al.*, in *Gravitational Waves, Proceedings of the Second Edoardo Amaldi Conference*, edited by E. Coccia *et al.* (World Scientific, Singapore, 1998), p. 148.
[17] J.-P. Zendri *et al.*, Class. Quantum Grav. **19**, 1925 (2002); for more information, see also http://www.auriga.lnl.infn.it.
[18] L. Conti *et al.*, Rev. Sci. Instrum. **69**, 554 (1998).
[19] L. Conti, M. De Rosa, and F. Marin, Appl. Opt. **39**, 5732 (2000).
[20] R. W. P. Drever, J. L. Hall, F. Kowalski, J. Hough, G. M. Ford, A. J. Mulney, and H. Ward, Appl. Phys. B: Photophys. Laser Chem. **31**, 97 (1983).
[21] L. Conti, Ph.D. thesis, University of Trento, 1999. Downloadable at the AURIGA web site: http://www.auriga.lnl.infn.it/publications/publications.html.
[22] L. Conti, M. De Rosa, and F. Marin, J. Opt. Soc. Am. B (to be published).
[23] M. De Rosa *et al.*, Class. Quantum Grav. **19**, 1919 (2002).
[24] P. R. Saulson, Phys. Rev. D **42**, 2437 (1990).
[25] E. Majorana and Y. Ogawa, Phys. Lett. A **233**, 162 (1997).
[26] K. Yamamoto, S. Otsuka, M. Ando, K. Kawabe, and K. Tsubono, Phys. Lett. A **280**, 289 (2001).
[27] L. Baggio *et al.*, Phys. Rev. D **61**, 102001 (2000), and references therein.
[28] See for instance A. Papoulis, *Probability, Random Variables, and Stochastic Processes*, 3rd ed. (McGraw-Hill, Singapore, 1991), p. 79.
[29] A. Ortolan, L. Baggio, M. Cerdonio, G. A. Prodi, G. Vedovato, and S. Vitale, Class. Quantum Grav. **19**, 1457 (2002).
[30] V. Crivelli-Visconti, A. Ortolan, L. Taffarello, G. Vedovato, M. Cerdonio, G. A. Prodi, and S. Vitale, Phys. Rev. D **57**, 2045 (1998).
[31] P. Astone *et al.*, Class. Quantum Grav. **19**, 1905 (2002).